

DETECTION OF A MAGNETIZED DISK AROUND A VERY YOUNG PROTOSTAR

RAMPRASAD RAO¹, JOSEP M. GIRART², SHIH-PING LAI^{3,4}, DANIEL P. MARRONE⁵

¹Institute of Astronomy and Astrophysics, Academia Sinica, 645 N. Aohoku Pl., Hilo, HI 96720, USA

²Institut de Ciències de l'Espai, (CSIC-IEEC), Campus UAB, Facultat de Ciències, C5p 2, 08193 Bellaterra, Catalonia; girart@ice.cat

³Institute of Astronomy and Department of Physics, National Tsing Hua University, Hsinchu 30013, Taiwan

⁴Academia Sinica Institute of Astronomy and Astrophysics, P.O. Box 23-141, Taipei 10617, Taiwan and

⁵Steward Observatory, University of Arizona, 933 North Cherry Avenue, Tucson, AZ 85721, USA

Draft version March 9, 2021

ABSTRACT

We present subarcsecond resolution polarimetric observations of the 878 μm thermal dust continuum emission obtained with the Submillimeter Array (SMA) towards the IRAS 16293–2422 protostellar binary system. We report the detection of linearly polarized dust emission arising from the circumstellar disk associated with the IRAS 16293–2422 B protostar. The fractional polarization of $\simeq 1.4\%$ is only slightly lower than that expected from theoretical calculations in such disks. The magnetic field structure on the plane of the sky derived from the dust polarization suggests a complex magnetic field geometry in the disk, possibly associated with a rotating disk that is wrapping the field lines as expected from the simulations. The polarization around IRAS 16293–2422 A at sub-arcsecond angular resolution is only marginally detected.

Subject headings: ISM: individual objects (IRAS 16293–2422) — ISM: magnetic fields — polarization — stars: formation — techniques: polarimetric

1. INTRODUCTION

The protostellar phase of star formation in a low mass star is thought to have the following structure: a deeply embedded protostar which is not observed directly, accompanied by an accretion (protoplanetary) disk, from where a powerful bipolar outflow is ejected, and further surrounded by a dense and warm envelope (Andre et al. 2000). The existence of rotationally supported disks in the earliest stages of the protostellar phase (Class 0 protostars) is a matter of debate (Jørgensen et al. 2009; Girart et al. 2009a; Tobin et al. 2013; Yen et al. 2013; Murillo & Lai 2013), since it is believed that magnetic braking can efficiently suppress the formation of a disk in the protostellar phase (e.g., Li et al. 2011).

IRAS 16293–2422 (henceforth I16293) is located in the ρ Ophiuchus cloud at a distance of 120 pc (e.g., Loinard et al. 2008). It is one of the most extensively studied low mass protostellar objects and powers a multiple outflow system (Walker et al. 1988; Mizuno et al. 1990; Rao et al. 2009; Loinard et al. 2013). At scales of a few hundred AU, the molecular emission shows two dense and warm condensations, sources IRAS 16293–2422 A (henceforth I16293A) and IRAS 16293–2422 B (henceforth I16293B), with a very rich chemical composition (Chandler et al. 2005; Takakuwa et al. 2007; Zapata et al. 2013). Very Large Array (VLA) observations at centimeter (cm) wavelengths show that I16293A has complex structure in the free-free emission (Wootten 1989; Mundy et al. 1992; Chandler et al. 2005), whereas the dust emission appears to be significant even at 1.3 cm for I16293B (Estalella et al. 1991; Loinard et al. 2007). VLA observations with an angular resolution of $0''.07$ at 7 mm show that the emission in I16293B arises from the dust and is well resolved, showing a clear disk-like morphology, which is possibly face-on (Rodríguez et al. 2005; Chandler et al. 2005; Loinard et al. 2013). I16293A is composed of

two compact sources, A1 and A2, separated by $\sim 0''.35$, surrounded by extended emission, but that emission arises primarily from free-free radiation (Pech et al. 2010; Loinard et al. 2013).

Aperture synthesis observations of the linearly polarized dust continuum emission at mm and submm wavelengths have been successful in revealing the magnetic field properties in dense cores at scales from few hundred to few thousand AU for both low and high mass star forming regions (Rao et al. 1998; Girart et al. 1999, 2006, 2009b; Lai et al. 2003; Tang et al. 2009; Hull et al. 2013). However, it has been more challenging to look for magnetic field signatures at circumstellar scales. Indeed, there have been a few attempts to detect the dust polarization from circumstellar disks with mm and submm arrays (CARMA and SMA). However, these have been unsuccessful with no positive detections but with stringent upper limits of $\simeq 0.5\%$ (Hughes et al. 2009, 2013). The authors explain that these non-detections are possibly due to inefficient grain alignment.

The earliest polarimetric observations toward I16293 were limited by low sensitivity (Flett & Murray 1991; Tamura et al. 1993; Akeson & Carlstrom 1997). Previous SMA observations at an angular resolution of $\sim 2''$ show that the large scale global direction of the field appears to lie along the dust ridge joining the two emission peaks. Yet, while I16293A is threaded by an “hourglass”-like magnetic field structure, I16293B, shows a relatively ordered magnetic field with no evidence of deformation (Rao et al. 2009). Circular and linear polarization have been detected in the 22 GHz water maser line around I16293A, with a derived total magnetic field strength of 110 mG (Alves et al. 2012). The water maser emission is probably arising in the interaction/shocked zoned of the outflow with the dense circumstellar gas.

In this letter, we present higher resolution SMA po-

larimetric observations of the continuum emission at 345 GHz toward I16293. The CO 3–2, SiO 8–7, C³⁴S 7–6 molecular line data of these observations have already been presented in a different paper (Girart et al. 2013), showing that at scales of few hundreds AU the outflow activity is centered in I16293A, with no clear indication of active outflow activity toward I16293B. Here, we report the first detection of the linear polarized dust thermal emission from a circumstellar disk, the one associated with I16293B.

2. OBSERVATIONS

The SMA observations were taken on 2010 August 28 in the extended configuration. The receiver was tuned to cover the 333.5–337.5 GHz and 345.5–349.5 GHz frequencies in the lower (LSB) and upper side band, (USB) respectively. The phase center of the telescope was RA(J2000.0)= 16^h23^m22^s.90 and DEC(J2000.0)= –24°28′35″.73 and all the maps presented in this paper are centered at this position. The gain calibrator was the QSO J1733–130. The bandpass and polarization calibrator was 3c454.3. The absolute flux scale was determined from observations of Neptune, with a flux uncertainty of ~ 20%. The data were reduced using the MIRIAD software package. The details of the polarization techniques and calibrations employed at the SMA are discussed in Marrone & Rao (2008) and Marrone et al. (2006). The instrumental polarization or “leakages” were found to be between 1 and 2% for the USB, while the LSB leakages were between 2 and 4%. These leakages were measured to an accuracy of 0.1%. Self-calibration was performed independently for the USB and LSB on the continuum emission from IRAS 16293–2422. This data from the extended configuration was combined with the data obtained in the compact configuration taken in April 2006, taking into account the proper motion of this region (Loinard et al. 2007). The results from the previous compact configuration observations have been reported by Rao et al. (2009). The combination resulted in maps with both greater sensitivity and greater dynamic range. All the maps were generated using natural weighting, which maximizes the sensitivity.

3. RESULTS AND ANALYSIS

The combined 878 μm dust map and the magnetic field distribution of the SMA extended and compact configurations resemble very well the maps reported by Rao et al. (2009, Fig. 1a and the bottom panel of their Fig. 2), in spite of the fact that the combined maps have a smaller beam (1″2) than the earlier maps (2″5). The dust continuum emission and the polarization detected using the combined data probably arise both from the envelope surrounding I16293A and I16293B, as well as from the putative compact, disk-like structures around these two objects (e.g., Rodríguez et al. 2005; Loinard et al. 2013). Henceforth, we try to approximately isolate the disk and envelope contributions.

In order to trace the putative circumstellar disks and resolve out the contribution from the envelope, we obtained maps excluding all the visibilities that have a radius lower than $r_{u,v}$. We generated maps with different values of $r_{u,v}$ (40, 60, 80, 100 and 120 k λ). The criterion used to define the radius ($r_{u,v}$) at which the emission arises mostly from circumstellar scales was the

Table 1
Properties of I16293A and I16293B

Component	Peak intensity (Jy Beam ⁻¹)	Flux density (Jy)	Size ^a
All I16293A	2.27 ± 0.04	6.30 ± 0.17	—
I16293B	2.69 ± 0.04	4.47 ± 0.24	—
Envelope component			
I16293A	1.08 ± 0.03	4.80 ± 0.18	3″12 × 1.56, 3°
I16293B	0.84 ± 0.03	2.30 ± 0.11	1″82 × 1.75, 88°
Compact component			
I16293A	0.79 ± 0.02	1.57 ± 0.07	1″03 × 0.10, 50°
I16293B	1.56 ± 0.02	1.98 ± 0.05	0″39 × 0.28, 80°

^a Deconvolved size and position angle

minimum value where the flux density does not change significantly, i.e. the rate of decrease of flux density with baseline length approaches zero. I16293B is an ideal test source since it has an accretion disk around the protostar (Rodríguez et al. 2005; Pineda et al. 2012; Zapata et al. 2013). Figure 2 shows the peak intensity and flux density of I16293B for different values of $r_{u,v}$. The flux and peak intensity decrease with $r_{u,v}$, but for $r_{u,v} \gtrsim 80$ k λ the decrease is minimal, indicating that most of the envelope has been resolved out. The map obtained with $r_{u,v} = 80$ k λ is shown in Figure 1c (a close-up toward I16293B is also shown in Fig. 3). To further test that most of the emission is associated with the disk, we have measured the source size and its flux. A Gaussian fit to I16293B gives a deconvolved size of 0″39 × 0″28 (47 AU × 34 AU, see Table 1). These values are consistent with previous measurements of the I16293B disk size (Rodríguez et al. 2005; Zapata et al. 2013). In addition, using the flux derived at 345 GHz from this map, 1.98 ± 0.05 Jy, and the flux measured from 0″2 angular resolution ALMA observations at 690 GHz (note that at this angular resolution ALMA detects only the disk, Loinard et al. 2013), 12.5 ± 0.5 Jy, the derived dust continuum spectral index is 2.67 ± 0.37 . This value is in agreement with the previous values measured in the centimeter to submillimeter wavelength range for the disk component (Rodríguez et al. 2005). Thus, most of the dust emission detected in the $r_{u,v} = 80$ k λ map is likely tracing the putative circumstellar disk around I16293B.

The polarized dust emission measured in the $r_{u,v} = 80$ k λ map, 0.02 Jy, is smaller than in the map obtained using all the visibilities, 0.12 Jy. Even though we have shown that the total dust emission in the $r_{u,v} = 80$ k λ map arises from the disk, it does not directly imply that the polarized emission arises only from the disk. The Stokes Q and U visibility response is quite different from the total emission. Thus, it is possible that the polarized emission may have some contribution from the envelope. To qualitatively test the possible envelope’s contribution we have generated artificial Stokes Q and U maps using a combination of positive and negative Gaussians with full width half maximum sizes of 1 – 4″. The criterion used for the artificial maps is that the polarized flux and the polarization pattern using all the visibilities is similar to the observed one as is shown in Figure 1a. These maps were converted into visibilities using the visibility coverage of our SMA observations. Then, we obtained synthetic SMA maps using all the visibilities, as well as using $r_{u,v} = 80$ and 120 k λ . We found that the artificial enve-

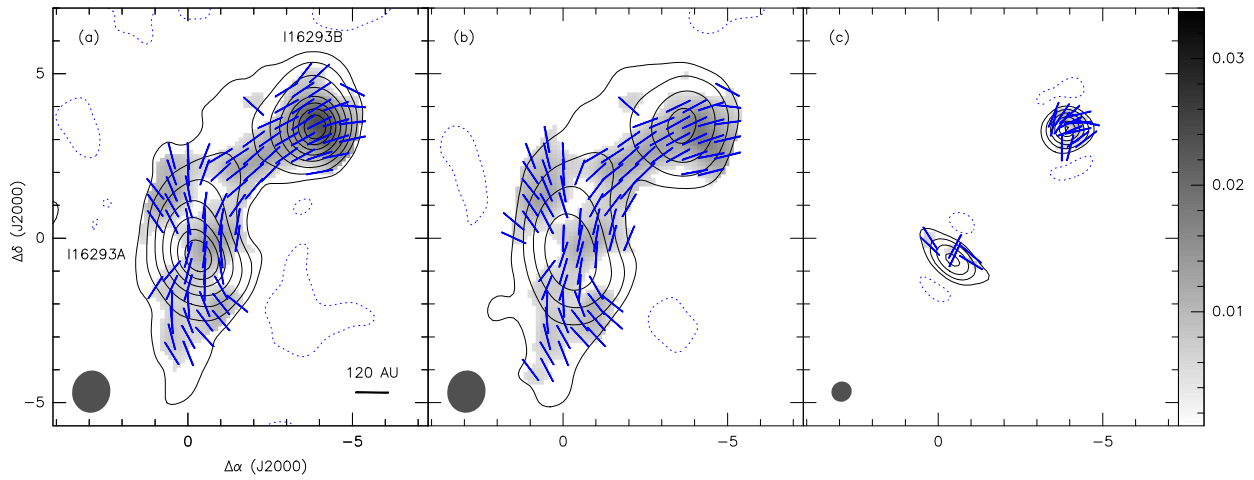


Figure 1. Composite of the contour maps of the $878 \mu\text{m}$ dust continuum emission, overlaid with the greyscale images of the polarized dust intensity and the magnetic field directions on the plane of the sky (blue segments) as derived from the polarized data. *Panel a:* Maps obtained using the combined SMA compact and extended configurations. *Panel b:* Maps for only the envelope contribution (obtained after subtracting the clean components of the map shown in panel c, see Section 3 for more details). *Panel c:* Maps obtained by using only baselines between 80 and 220 $k\lambda$. For all the panels the contour levels are $-0.08, 0.08, 0.2, 0.4, 0.7, 1.1, 1.5, 1.9$ and 2.3 Jy Beam^{-1} and the grey scale is the same. The wedge on the right of the c panel shows the polarized intensity scale in Jy Beam^{-1} . The synthesized beams are shown in the bottom-left corner of each panel: The beam's full width at half maximum (FWHM) and its position angle are $1''.29 \times 1''.16$ and -10.8° for the a and b panels, and $0''.63 \times 0''.61$ and -40.0° for the c panel (these resolutions imply a spatial resolution of 146 AU and 75 AU, respectively).

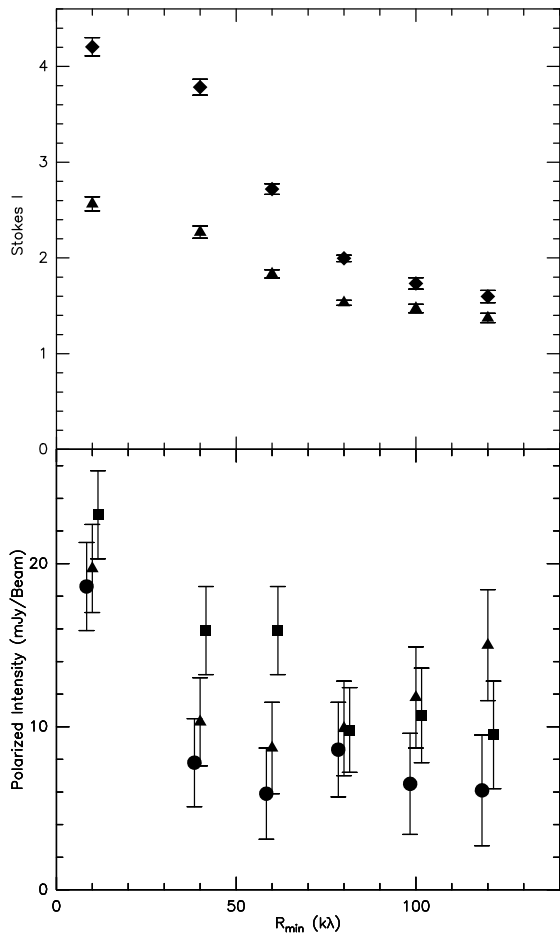


Figure 2. *Panel a:* Dust continuum 878 μm emission around I16293B as a function of $r_{u,v}$ in units of $k\lambda$ (see Section 3 for the definition of this parameter). Filled rhombus and triangle show the total flux and peak intensity, respectively. *Panel b:* Polarization intensity for 3 different positions in I16293B as a function of $r_{u,v}$. These positions are marked in Fig. 3a.

lope’s polarization detected in the $r_{u,v}=80$ and 120 $k\lambda$ maps, 4 and 2 mJy Beam^{-1} respectively, is smaller than the measured value toward I16293B, 10 mJy Beam^{-1} . Moreover, while the artificial envelope’s polarized flux clearly decreases between $r_{u,v}=80$ and 120 $k\lambda$, the observed one remains constant. In Figure 2b, we show, for the different $r_{u,v}$ maps, the polarized flux measured at three different positions within I16293B. Thus, although we cannot discard definitively the fact that the 80 $k\lambda$ polarization maps have some residual envelope contribution, it seems that most of the polarization detected arises probably from the disk. Interestingly, the polarization seems to arise from a remarkable partial ring structure (see Figure 3). The magnetic field derived from the dust polarization has a different morphology than the one associated using all the visibilities.

The $r_{u,v}=80$ $k\lambda$ map (Fig. 1c) shows that the dust emission around I16293A is elongated in the NE-SW direction ($\text{PA}\simeq 50^\circ$) with a major axis of $\simeq 120$ AU (see Table 1). The direction of the elongation is similar to what has been found previously (Loinard et al. 2013; Girart et al. 2013). However, the size measured is smaller than the rotating molecular structure observed with the C^{34}S 7-6 line (diameter of 280 AU), which is likely tracing a rotating circumbinary disk around

sources A1 and A2 (Girart et al. 2013). This suggests that we are resolving partially the emission of this structure. The dust polarization associated with I16293A shows only three weak patches of emission, the magnetic field direction in two of them is along the disk axis and in the other it is perpendicular. However, since the emission is patchy and the significance of these detections is more marginal than those toward I16293B, we focus the discussion on I16293B.

To obtain the map with the envelope contribution only, the clean components of the $r_{u,v}=80$ $k\lambda$ map (Fig. 1c) were subtracted from the original visibilities for both the compact and extended array data (e.g., Frau et al. 2011). The data from the two sidebands and from each array configuration were treated separately when doing the subtraction. The map obtained using the resulting visibilities is shown in Figure 1b. The map showing just the envelope contribution looks similar to the map using all the data, with the difference that the envelope emission is considerably smoother (i.e., not as strongly peaked) in I16293A, and significantly more so in I16293B. Table 1 shows the measured flux density, peak intensity and size of the envelope contribution. About 76% and 51% of the total flux measured in I16293A and I16293B, respectively, arises from the envelope. The envelope is slightly smaller in I16293B ($1''.8$ or 210 AU) than in I16293A ($2''.2$ or 260 AU). The continuum flux of I16293B is also smaller, by a factor $\simeq 2$, than that of I16293A. This suggests that if the temperatures in the envelope are not too different, the mass of the envelope in I16293B is a factor 2 smaller than the envelope mass in I16293A. Interestingly, the overall pattern of the magnetic field of the envelope also resembles well the pattern obtained using all the data. In addition, the polarized flux from the envelope (0.11 Jy) is similar to that measured using all the data (0.12 Jy). This suggests that using all the visibilities from the compact and extended configurations, the magnetic field traced is dominated by the contribution from the envelope. The contribution to the polarized flux from the disk arises from a much smaller area when compared to the contribution from the envelope.

4. DISCUSSION AND CONCLUSIONS

In the previous section, we have shown that the 878 μm total and polarized dust emission map obtained with a $r_{u,v}$ of 80 $k\lambda$ (Fig. 3a) is likely tracing the previously reported circumstellar disk around I16293B. The magnetic field pattern derived from the dust polarization and associated with the disk (Fig. 1c) appears to be distinct from the field structure as seen in the envelope (Fig. 1b). And indeed, the magnetic field direction appears to rotate along the ring i.e., azimuthally. Only the vectors in the South-West section of the ring depart from this general trend. This is suggestive of a toroidal magnetic field that is being wrapped by the rotation of the disk (Hennebelle & Ciardi 2009; Kataoka et al. 2012). As a qualitative comparison, Figure 3b shows the synthetic map of the expected magnetic field pattern in a rotating circumstellar disk with a face-on configuration for the case of a low mass protostar located at 140 pc, and thus is at a distance not too different from our target, obtained by Padovani et al. (2012). Interestingly, the I16293B magnetic field pattern roughly resembles the expected configuration for a magnetized rotating, disk.

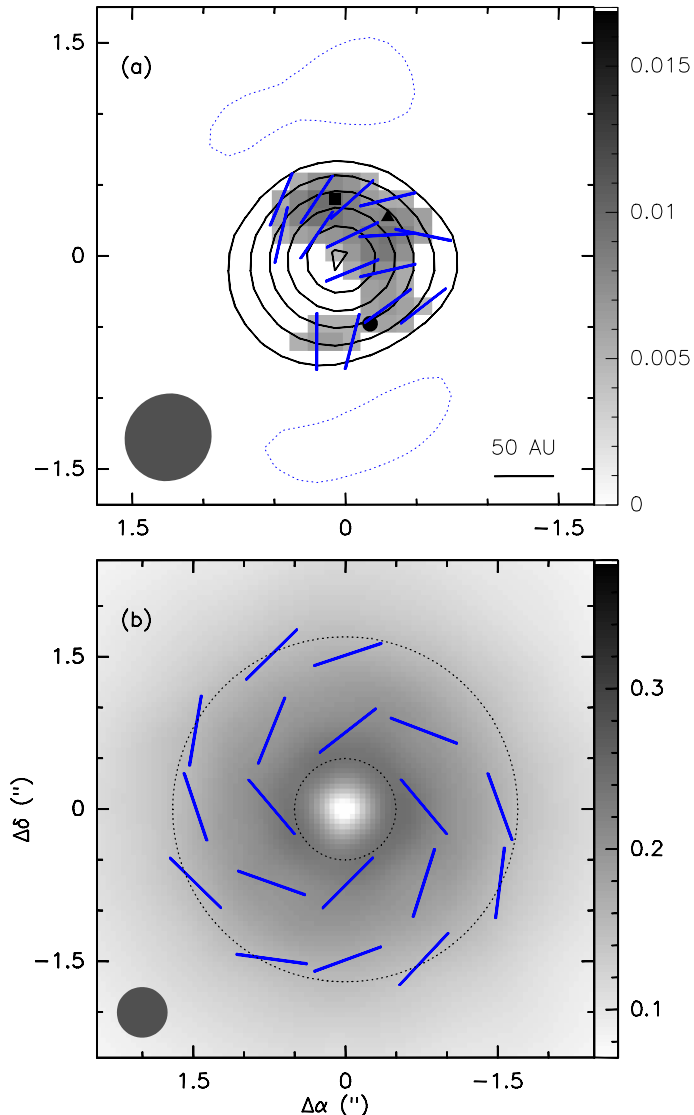


Figure 3. *Panel a:* A close up of Figure 1c toward I16293B. The filled triangle, square and circle show the selected position shown in Figure 2b. These positions are separated between $0''.40$ and $0''.76$ (the beam’s FWHM is $0''.61$). *Panel b:* Synthetic map of the linearly polarized dust emission (grey scale), magnetic field direction (blue segments) and the dust emission (dotted lines). This map has been adapted from the Figure 8 of Padovani et al. (2012). It shows the magnetic field at circumstellar disk scales derived for a collapsing magnetized dense core located at a distance of 140 pc and at time of collapse of 1.94×10^4 yr (Hennebelle & Fromang 2008; Hennebelle & Ciardi 2009). The total and polarized dust emission of the synthetic maps are in an arbitrary scale and are shown for qualitative analysis.

Theoretical studies of magnetized cores show that it is very difficult to form a circumstellar disk in the earliest stages of the collapse (e.g., Krasnopolsky et al. 2010; Machida & Matsumoto 2011; Li et al. 2011). This is because magnetic braking is so effective that only a very small, observationally undetectable, disk can be formed around the protostar (Dapp et al. 2012). Only at later stages, when the surrounding envelope becomes less massive, magnetic braking becomes inefficient, allowing a circumstellar disk to grow (Machida et al. 2011). Nevertheless, other simulations show that when rotation and magnetic field axis are misaligned, then magnetic braking can be inefficient, and for large misalignments a relatively

massive circumstellar disk is formed in the protostellar phase (Joos et al. 2012). For the case of I16293B, the data presented here suggests that this source has a more diffuse envelope than I16293A: on one hand the flux density (and therefore likely its mass) of the I16293B envelope is a factor 2 lower than in the I16293A envelope; on the other hand, 50% of the flux measured toward I16293B using the compact and extended configurations is detected in the $r_{u,v} = 80$ k λ map, whereas this fraction in I16293A is only 25%. Therefore, it appears that a higher fraction of the I16293B envelope has already accreted into the disk and protostar than in I16293A. This suggests that, as proposed by theory, the well formed I16293B magnetized disk is due to the fact that I16293B is probably more evolved than I16293A. Further evidence supporting this argument stems from the lack of outflow activity in I16293B, when compared to I16293A (Rao et al. 2009; Alves et al. 2012; Girart et al. 2013).

Previous observations of circumstellar disks failed to detect the polarized dust emission down to stringent upper limits, $\lesssim 0.5\%$, (Krejny et al. 2009; Hughes et al. 2009, 2013). These upper limits are well below the $\simeq 2\text{--}3\%$ polarization fractions expected from simulations of a magnetized circumstellar disk (i.e., having a predominantly toroidal magnetic field) with standard dust grain alignments (Cho & Lazarian 2007). These results have been interpreted either due to inefficient alignment of large grains, or insufficient magnetic field strength for alignment, or as a consequence of magnetic field tangling by turbulent motions (Hughes et al. 2013). The polarization fractions detected toward the I16293B disk are in the 0.5–3.0%, with a median value of 1.4%. These values are above the upper limits obtained previously in other YSOs, but slightly below the predicted values from the theory. For a better comparison with the expected polarization properties, observations at higher angular resolution and sensitivity are definitively needed. It is worth noting that the sample used in previous observations are from YSOs significantly more evolved than I16293B, as they are classical T Tauri or HAeBe stars (HD 163296, TW Hydra, GM Aur, DG Tau and MWC 480: Krejny et al. 2009; Hughes et al. 2009, 2013). Thus, we speculate that the polarization efficiency decreases with time, either due to a loss of alignment efficiency or by other causes.

In summary, we report the first detection of linearly polarized dust emission in a circumstellar disk around a young stellar object from SMA observations made at submillimeter wavelengths. The magnetic field configuration roughly resembles that from a rotating disk with the toroidal field lines being wrapped by the rotating gas and dust, forming a spiral pattern. Clearly, the significant improvement in the sensitivity and image quality that ALMA provides will allow us to better sample the magnetic field geometry in the I16293B disk, and to map the magnetic field structure in the I16293A circumbinary disk.

The Submillimeter Array is a joint project between the Smithsonian Astrophysical Observatory and the Academia Sinica Institute of Astronomy and Astrophysics. We thank all members of the SMA staff that made these observations possible. JMG also thanks the

SMA staff at Hilo for their support. JMG is supported by the Spanish MINECO AYA2011-30228-C03-02 and Catalan AGAUR 2009SGR1172 grants. SPL acknowledges support from the National Science Council of Taiwan with Grants NSC 98-2112-M-007-007-MY3, NSC 101-2119-M-007-004, and 102-2119-M-007-004-MY3.

REFERENCES

- Akeson, R. L., & Carlstrom, J. E. 1997, *ApJ*, 491, 254
 Alves, F. O., Vlemmings, W. H. T., Girart, J. M., & Torrelles, J. M. 2012, *A&A*, 542, A14
 Andre, P., Ward-Thompson, D., & Barsony, M. 2000, *Protostars and Planets IV*, 59
 Chandler, C. J., Brogan, C. L., Shirley, Y. L., & Loinard, L. 2005, *ApJ*, 632, 371
 Cho, J. & Lazarian, A. 2007, *ApJ*, 669, 1085
 Dapp, W. B., Basu, S., & Kunz, M. W. 2012, *A&A*, 541, A35
 Estalella, R., Anglada, G., Rodríguez, L. F., & Garay, G. 1991, *ApJ*, 371, 626
 Flett, A. M., & Murray, A. G. 1991, *MNRAS*, 249, 4P
 Frau, P., Galli, D., & Girart, J. M. 2011, *A&A*, 535, A44
 Girart, J. M., Beltrán, M. T., Zhang, Q., Rao, R., & Estalella, R. 2009, *Science*, 324, 1408
 Girart, J. M., Rao, R., & Estalella, R. 2009, *ApJ*, 694, 56
 Girart, J. M., Crutcher, R. M., & Rao, R. 1999, *ApJ*, 525, L109
 Girart, J. M., Estalella, R., Palau, A., Torrelles, J. M., & Rao, R. 2013, *ApJ*, in press, arXiv:1311.4745
 Girart, J. M., Rao, R., & Marrone, D. P. 2006, *Science*, 313, 812
 Hennebelle, P., & Ciardi, A. 2009, *A&A*, 506, L29
 Hennebelle, P., & Fromang, S. 2008, *A&A*, 477, 9
 Hughes, A. M., Hull, C. L. H., Wilner, D. J., & Plambeck, R. L. 2013, *AJ*, 145, 115
 Hughes, A. M., Wilner, D. J., & Cho, J. et al. 2009, *ApJ*, 704, 1204
 Hull, C. L. H., Plambeck, R. L., Bolatto, A. D., et al. 2013, *ApJ*, 768, 159
 Joos, M., Hennebelle, P., & Ciardi, A. 2012, *A&A*, 543, A128
 Jørgensen, J. K., van Dishoeck, E. F., Visser, R., et al. 2009, *A&A*, 507, 861
 Kataoka, A., Machida, M. N., & Tomisaka, K. et al. 2012, *ApJ*761, 40
 Krasnopolsky, R., Li, Z.-Y., & Shang, H. 2010, *ApJ*, 716, 1541
 Krejny, M., Matthews, T., & Novak, G. et al. 2009, *ApJ*705, 717
 Lai, S.-P., Girart, J. M., & Crutcher, R. M. 2003, *ApJ*, 598, 392
 Li, Z.-Y., Krasnopolsky, R., & Shang, H. 2011, *ApJ*, 738, 180
 Loinard, L., Chandler, C. J., Rodríguez, L. F., et al. 2007, *ApJ*, 670, 1353
 Loinard, L., Torres, R. M., Mioduszewski, A. J., & Rodríguez, L. F. 2008, *ApJ*, 675, L29
 Loinard, L., Zapata, L. A., Rodríguez, L. F., et al. 2013, *MNRAS*, 430, L10
 Machida, M. N., & Matsumoto, T. 2011, *MNRAS*, 413, 2767
 Machida, M. N., Inutsuka, S.-I., & Matsumoto, T. 2011, *PASJ*, 63, 555
 Marrone, D. P., Moran, J. M., Zhao, J.-H., & Rao, R. 2006, *ApJ*, 640, 308
 Marrone, D. P., & Rao, R. 2008, *Proc. SPIE*, 7020
 Mizuno, A., Fukui, Y., Iwata, T., Nozawa, S., & Takano, T. 1990, *ApJ*, 356, 184
 Mundy et al. 1992, *ApJ*, 385, 306
 Murillo, N. M., & Lai, S.-P. 2013, *ApJ*, 764, L15
 Padovani, M., Brinch, C., Girart, J. M., et al. 2012, *A&A*, 543, A16
 Pech, G., Loinard, L., Chandler, C. J., et al. 2010, *ApJ*, 712, 1403
 Pineda, J. E., Maury, A. J., Fuller, G. A., et al. 2012, *A&A*, 544, L7
 Rao, R., Crutcher, R. M., Plambeck, R. L., & Wright, M. C. H. W. 1998, *ApJ*, 502, L98
 Rao, R., Girart, J. M., Marrone, D. P., Lai, S.-P., & Schnee, S. 2009, *ApJ*, 707, 921
 Rodríguez, L. F., Loinard, L., D'Alessio, P., Wilner, D. J., & Ho, P. T. P. 2005, *ApJ*, 621, L133
 Tamura, M., Hayashi, S. S., Yamashita, T., Duncan, W. D., & Hough, J. H. 1993, *ApJ*, 404, L21
 Tang, Y.-W., Ho, P. T. P., Girart, J. M., Rao, R., Koch, P., & Lai, S.-P. 2009, *ApJ*, 695, 1399
 Takakuwa, S., et al. 2007, *ApJ*, 662, 431
 Tobin, J. J., Hartmann, L., Chiang, H., et al. 2013, *ApJ*, 771, 41
 Walker, C. K., Lada, C. J., Young, E. T., & Margulis, M. 1988, *ApJ*, 332, 335
 Wootten, A. 1989, *ApJ*, 337, 858
 Yen, H.-W., Takakuwa, S., Ohashi, N., & Ho, P. T. P. 2013, *ApJ*, 772, 22
 Zapata, L. A., Loinard, L., Rodríguez, L. F., et al. 2013, *ApJ*, 764, L14